Effect of FEC electrolyte additive on the electrochemical performance of nickel-rich NCM ternary cathode

Shengxian She[1,#], Yangfan Zhou[1,#], Zijian Hong[1, 2, 3*], Yuhui Huang[1, 3], Yongjun Wu [1, 2,*]

[1] School of Materials Science and Engineering, Zhejiang University, Hangzhou 310027, China

[2] Cyrus Tang Center for Sensor Materials and Applications, State Key Laboratory of Silicon Materials, Zhejiang University, Hangzhou, Zhejiang 310027, China

[3] Research Institute of Zhejiang University-Taizhou, Taizhou, Zhejiang 318000, China

*Email: hongzijian100@zju.edu.cn (Z. H.); yongjunwu@zju.edu.cn (Y. W.)

[#] Contributed equally

Abstract

It has been well established recently that fluorinated electrolyte additives such as Fluoroethylene carbonate (FEC) could promote the formation of LiF-based solid electrolyte interphase that can stabilize lithium metal anode. Meanwhile, the impact of FEC additive on the cathode side, particularly for the high energy density nickel-rich $LiNi_{1-x-y}Co_xMn_yO_2$ (NCM) ternary cathodes, remains unclear. In this study, we investigated the structural and chemical composition of cathode electrolyte interphase

(CEI) and its electrochemical performance to elucidate the effect of FEC additive on the $LiNi_{0.9}Co_{0.05}Mn_{0.05}O_2$ (NCM90) cathode for high energy lithium-ion batteries. It is discovered that the FEC additive in carbonate electrolyte (BE-FEC) can produce LiF-based CEI, which could stabilize the NCM90 surface and improve the cycle performance at low cut-off voltage. While the formation of a thick LiF layer under high cut-off voltage and high rate leads to a higher polarization and slower Li+ transport kinetics, which in turn deteriorates the battery performance. Whereas in carbonate electrolyte (BE), under low voltage, the unstable Li_2CO_3-based amorphous CEI components form on the NCM90 surface while an intermediate rock salt structure can also be identified, leading to poor cycle life. While under high voltage, the BE sample shows superior electrochemical performance due to the formation of a thin LiF layer from the decomposition of the $LiPF_6$. Our work provides a comprehensive understanding of the role of FEC in the CEI of nickel-rich cathodes, offering practical guidance for the design of electrolytes for high-energy nickel-rich cathodes.

Keywords

Introduction

The Lithium-ion battery is one of the most successful energy storage systems for the past three decades, which has emerged as a cornerstone for our modern civilization[1-3]. The electrolyte between a cathode and an anode is an indispensable component in a lithium-ion battery.[4-8] It not only transports Li-ions in the cell during the charge/discharge process, but also leads to the formation of complex interfaces on the electrodes (i.e., solid electrolyte interface, SEI, or cathode electrolyte interface, CEI) that could play an essential role in determining battery performances. Carbonate-based (e.g., ethylene carbonate/ dimethyl carbonate, EC/DMC) electrolytes have achieved great success due to their excellent Li^+ transport property and good stability, which have become the mainstream commercial electrolytes.[7-9] However, the SEI formed with carbonate-based electrolytes is mainly composed of carbonate ionic phase (e.g., lithium carbonate, Li_2CO_3), organic lithium compounds (e.g., lithium ethylene decarbonate), and other organic species, which usually has poor stability.[10-12]

To improve the properties of the electrode-electrolyte interphases, in particular, the anode surface, a widely used strategy is to add one or multiple electrolyte additives to form stable artificial SEI compositions that could suppress further side reactions between the electrolyte and anode as well as the growth of the notorious lithium dendrites.[13, 14] For instance, fluorinated carbonates (e.g., fluoroethylene carbonate, FEC) are widely used as electrolyte additives, which could produce LiF (an SEI component with high mechanical strength and good ion transport properties) on the lithium metal anode surface.[15-17] While tremendous previous reports have demonstrated that addition

of the fluorinated carbonates could improve the electrochemical performance of lithium metal batteries, the effect of fluorinated additives on the cathode, has not been fully understood.

Nickel-rich ternary cathodes $LiNi_xCo_yMn_{1-y-x}O_2$ (NCM, x≥0.8) with a high specific capacity, high operation voltage, and high specific energy density have been envisioned as promising cathode materials for the next generation power systems, e.g., in electric vehicles.[18-20] However, the poor cycle stability at high voltage has been a key obstacle to the full commercialization of the nickel-rich ternary cathodes. Two intriguing questions to ask: What are the main CEI components for nickel-rich ternary cathodes with fluorinated electrolyte additives? Can fluorinated electrolyte additives such as fluorinated carbonates help stabilize the nickel-rich ternary cathodes?

Herein, we employ the FEC electrolyte additive with commercially available EC/DMC electrolyte and $LiNi_{0.9}Co_{0.05}Mn_{0.05}O_2$ (NCM90) cathode as an example to investigate the effect of fluorinated electrolyte additives on nickel-rich NCM ternary cathode. The phase transitions, interface compositions and structures, electrochemistry, and cycle performances are studied with two types of electrolytes, baseline electrolyte (abbreviated as BE, EC/DMC 1:1 in volume ratio) and that with FEC additive (abbreviated as BE-FEC). Ex-situ X-ray diffraction (ex-situ XRD) and high-resolution transmission microscopy (HRTEM) indicate that NCM90 in BE undergoes phase transition with a larger volume change, leading to the formation of an intermediate rock-salt phase between the surface and bulk. X-ray photoelectron spectroscopy (XPS) shows that more LiF is generated in BE-FEC as expected due to the reaction of FEC

additive with NCM cathodes. Electrochemical impedance spectroscopy (EIS), galvanostatic intermittent titration technique (GITT), and cyclic test further showed the addition of FEC hinders the diffusion kinetics of Li^+ at the interface. Based on this work, we found that the extra LiF produced by FEC decomposition could inhibit the irreversible phase transition of NCM90 at the high de-lithiation state, thus suppressing the degradation of NCM90 during cycling. However, the inclusion of LiF in CEI can potentially obstruct the movement of Li^+ and augment the polarization at the interface, thereby constraining the discharge capacity of the cathode material with high charge/discharge voltage. We hope this study to spur further interest in the understanding of complex surface reactions between electrolyte additives and cathode materials, as well as the design of better battery systems with an in-depth understanding of the CEI compositions and their failure mechanisms.

Results

Detailed experimental procedures can be found in the **Experimental section**. **Fig. 1** shows the structural characterizations of the NCM90 cathodes at different de-lithiation stages after cycling twice. Ex-situ XRD patterns for charged and discharged NCM90 cathodes in BE are shown in Fig. 1(a), the diffraction pattern of the current collector, Al@C foil, is marked as the baseline. The main diffraction peaks of the NCM ternary cathode are observed during cycling, whereas a shift of the diffraction peak near 20° can be discovered. The diffraction peak near 20° corresponds to the (003) crystal plane, which is further highlighted in Fig. 1(b). During the charging process, a left shift of the peak can be found with the increasing of the cell voltage, indicating the expansion

of the lattice constant c during deintercalation. When the voltage increases above 4.25 V, the (003) diffraction peak shifts towards a higher degree dramatically, which can be attributed to the structural reconstruction at high voltage after higher degrees of de-lithiation.[21-23] This process is reversible, where the crystal structure can be restored after discharging to below 4.25 V. Further decreasing of the voltage during discharging leads to the decreasing of the lattice constant c. Meanwhile, a shift of the diffraction peaks is subtle for the BE-FEC as compared to BE, as depicted in Fig. 1(c). Zoom-in of the (003) diffraction peak (Fig. 1d) shows a similar trend with the BE electrolyte, however, the sudden decrease of the lattice constant c at higher voltages is absent for BE-FEC. This suggests that the addition of FEC can stabilize the NCM90 particles at high voltage. To get a direct comparison, both in-plane (a) and out-of-plane (c) lattice constants are plotted as a function of the voltage (Fig. 1e-1f). It is clearly shown that the lattice constant a decreases at high voltage (with less lithium below 4.25 V) for both electrolytes. Notably, for BE-FEC, a slight increase in the lattice constant a can be observed above 4.25 V. A maximum lattice shrinkage of ~2.3% can be found with the BE electrolyte. The lattice constant c increases slightly with increasing voltage below 4.25 V for both cases, while a sudden decrease by ~7 % can be seen when charging to 4.6 V with BE electrolyte, as has been discussed before. It can be concluded that with the FEC additive, the NCM90 is relatively stable during cycling with a lattice change of ~2 % while a large structural reconstruction at high voltage can be seen with the conventional commercialized carbonate electrolyte. Interestingly, this structural reconstruction is fully reversible where the structure can be fully restored for the

consequent cycles.
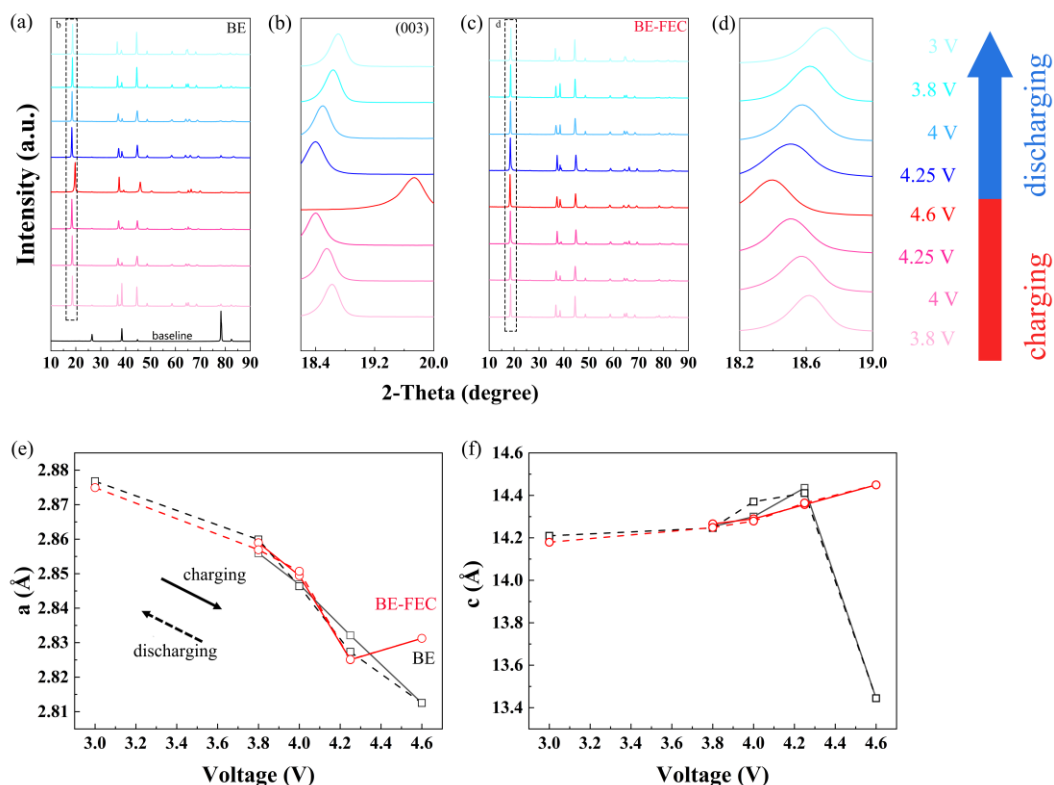
Fig. 1. XRD patterns for NCM90 holding at different charging/discharging voltage in (a)BE and (c)BE-FEC at the third cycle. The diffraction peak of (003) plane is shown in (b) and (d), respectively. The lattice parameter of (e) **a** and (f) **c** is derived from XRD patterns.

HRTEM characterizations were performed to investigate the surface structure of the NCM90 cathode materials cycled in BE and BE-FEC after 150 cycles with a cut-off voltage of 4.25 V, as shown in **Fig. 2**. An ordered lattice fringe structure can be seen in the bulk crystal for both samples (region I), with a lattice plane distance of ~4.97 Å. Selected fast Fourier transform (FFT) patterns of the region I confirm the formation of a typical layered structure, consistent with previous reports.[24, 25] For NCM90 cycled in BE, two more phases can be identified from Fig. 2(a), an amorphous phase layer with

a width of ~3.2 nm forms near the interface, (from the blue dotted line to the surface),
followed by a double-layer structure of rock salt phase (~8.1 nm, between red and blue
dotted line) between the amorphous layer and the bulk region. The formation of an
intermediate rock salt phase has also been reported in previous literature.[26, 27]
Meanwhile, when cycled in BE-FEC, a mix of the amorphous components and residual
layered phase with a width of ~10 nm (from the blue dotted line to the surface) can be
discovered at the interface. The formation of the interfacial rock-salt layer in BE is
mainly due to the high voltage charge/discharge process, where the large structural
reconstruction is not fully reversible after 150 cycles, while the lower oxidation
potential of fluorinated additive FEC is responsible for the formation of thicker
amorphous CEI layer, which also helps to stabilize the layered structure.
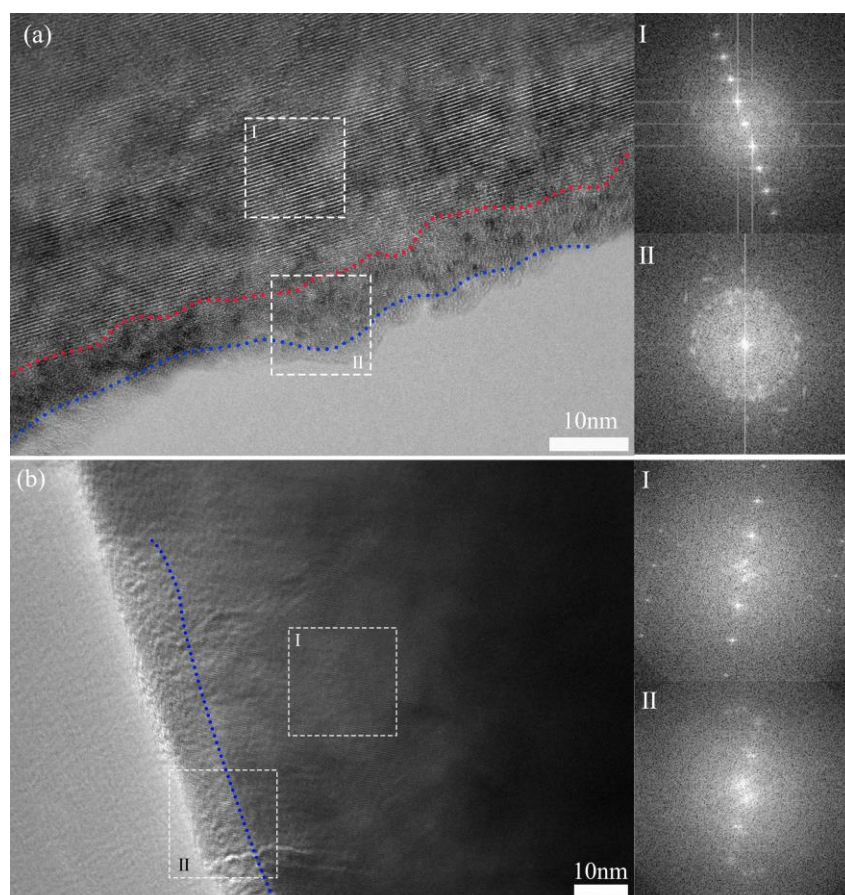
Fig. 2. HRTEM images and FFT patterns for bulk and surface section of NCM90 cycled in (a)BE and (b)BE-FEC for 150 cycles.

To determine the chemical components of surface CEI formed in both electrolytes, XPS measurements were performed (**Fig. 3**). The C 1s and F 1s XPS spectra of NCM90 cathode cycled in BE and BE-FEC for 1 cycle and 100 cycles within 2.5-4.25 V and 2.5-4.6 V are plotted. With a cut-off voltage of 4.25 V (**Fig. 3a**), the XPS peak of Li_2CO_3 is more significant for the BE sample as compared to BE-FEC. Li_2CO_3 is a typical CEI component, which exists on the NCM cathode surface due to the reaction with CO_2 in the air during production and storage. While the extra Li_2CO_3 signal in BE sample can be attributed to the decomposition of carbonate electrolyte during cycling. A slight decrease in the Li_2CO_3 signal can be found after 100 cycles for both samples, which indicates that the Li_2CO_3-based CEI is relatively unstable during cycling. For the F 1s spectra, the signal of $PVDF/Li_xPO_yF_z$ dominates for the BE sample, while a relatively smaller LiF peak at 686 eV can also be discovered. Whereas for the BE-FEC sample, the signal of LiF is more significant after even 1 charge/discharge cycle. This indicates that under a relatively low charge potential, with very little $LiPF_6$ decomposition, LiF in CEI is mainly generated from the decomposition of fluorinated additive FEC for the BE-FEC sample. No large changes in intensity can be observed for the LiF peaks after 100 cycles for both samples. This implies that the surface LiF is relatively stable as compared to the other CEI components such as Li_2CO_3 at a relatively lower voltage below 4.25 V.

As the cut-off potential increases to 4.6 V, the Li_2CO_3 peak area of the BE sample

is relatively larger than that of the BE-FEC sample (**Fig. 3b**). Meanwhile, a slight increase in the Li_2CO_3 peak area can be seen after 100 cycles for both BE and BE-FEC samples, suggesting that the continuous decomposition of the electrolytes and reactions with the NCM90 surface at higher voltages. The F 1s spectra of the BE sample after 1 cycle are quite similar to the case with the lower voltage of 4.25 V. However, a dramatic increase in the LiF signal after 100 cycles is clearly shown with BE. This can be attributed to the decomposition of the $LiPF_6$ salt and conversion of the $PVDF/Li_xPO_yF_z$ CEI components to LiF at a higher charging potential. Increasing the charge potential also affects the F 1s spectra of the BE-FEC sample, as shown in Fig. 3(b). The relative magnitude of the LiF peak is similar to the $PVDF/Li_xPO_yF_z$ peak, which means the $LiPF_6$ decomposition also changes the distribution of F species on the NCM90/BE-FEC interface. While after 100 cycles, the LiF peak is more significant, indicating that the further decomposition of the BE-FEC electrolyte leads to the formation of LiF-based CEI. Interestingly, overall, the existence of FEC can inhibit Li_2CO_3 generation, under both high and low voltage.

In a short discussion, it can be found that at low potential with commercialized electrolyte, Li_2CO_3-based CEI components are formed, which are unstable during cycling. At high potential, the decomposition of $LiPF_6$-based salt could lead to the formation of LiF-based stable CEI components for BE. Meanwhile, the addition of FEC facilitates the formation of LiF-based CEI components while suppressing the formation of Li_2CO_3, even at low potential.
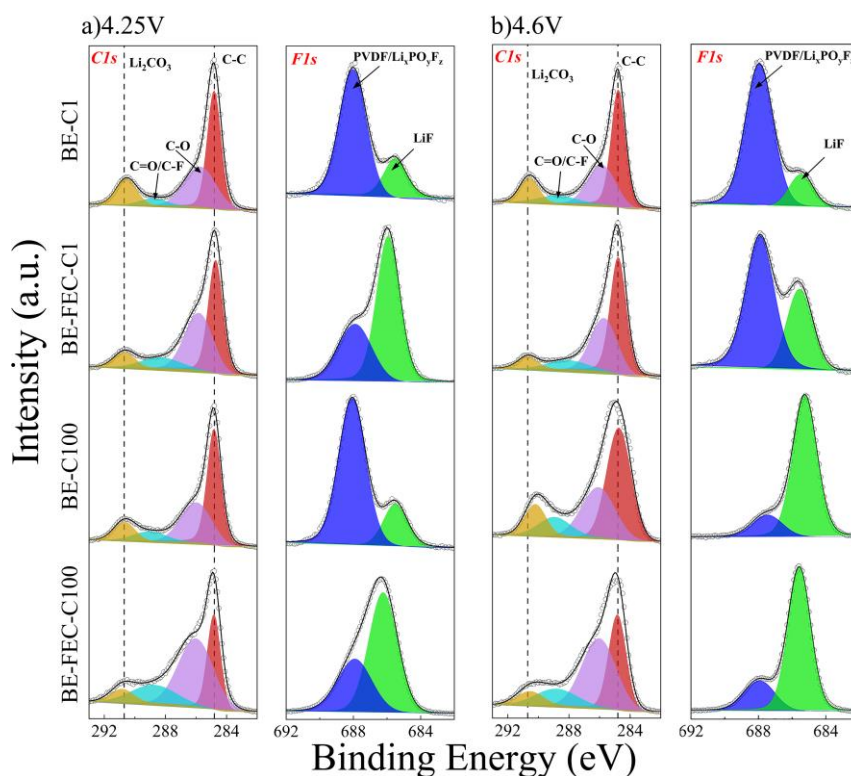
Fig. 3. C 1s and F 1s XPS spectra of NCM90 cathode cycled in BE and BE-FEC charging/discharging for 1 cycle and 100 cycles within (a) 2.5-4.25 V and (b) 2.5-4.6 V. From top to bottom, 1 cycle in BE; 1 cycle in BE-FEC; 100 cycles in BE; 100 cycles in BE-FEC.
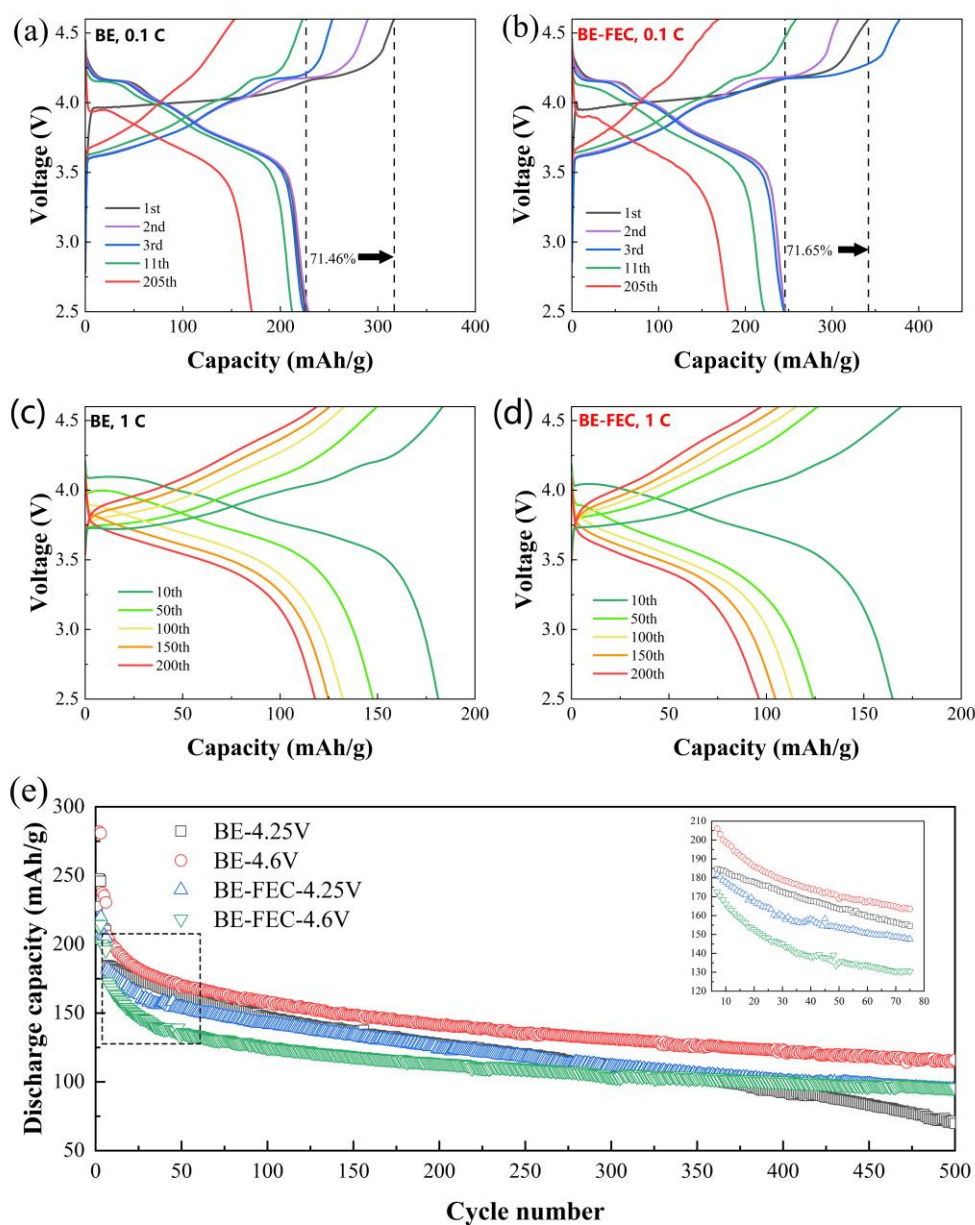
The charge/discharge voltage profiles of the NCM90 cell during cycling between 2.5 V to 4.6 V are depicted in **Fig. 4** and **Fig. S1**. Fig. 4(a) and 4(b) show voltage profiles at a low rate (0.1 C) interspersed between ordinary 1 C cycles with BE and BE-FEC, respectively. The charge plateau between 3.6 V to 4.25 V can be observed for both samples, consistent with literature reports.[28, 29] The coulombic efficiency of the first cycle is very similar for both BE and BE-FEC cells, while the discharge capacity of the BE-FEC cell (~245 mAh/g) is much higher than that of BE cell (~225 mAh/g) for the first cycle. This indicates that the stable LiF-based CEI can protect the cathode material

from cracking and prevent Li dissolution. The BE-FEC sample shows a slightly higher discharge capacity after 205 cycles (~10% higher in discharge capacity). While for the batteries cycled at a1 C rate, the voltage profiles for the 10th, 50th, 100th, 150th, and 200th cycles are shown in Fig. 4(c) and 4(d) for the two samples. It can be found that the charge voltage plateau increases to 3.75 V~4.25 V, due to the increasing polarization at a higher C-rate. The starting voltage of discharging platform is substantially lower for BE-FEC at 1 C rate (~0.15 V at 200th cycle), which can be attributed to the formation of thicker insulating LiF. The charge/discharge capacity decreases for both samples at 1 C during cycling, while as compared to BE, the discharge capacity of NCM90 drops faster in BE-FEC. After 200 cycles, the discharge capacity for the BE sample is 26% higher than BE-FEC (~120 mAh/g for BE sample vs. ~95 mAh/g for BE-FEC). **Fig. S2** further shows the differential capacity curves of NCM90 cells with BE and BE-FEC at both 0.1 C and 1 C rates. Three obvious peaks can be observed from primary charging curves at 0.1 C (especially from 3rd cycle). The peak positions are almost identical for the BE and BE-FEC samples. After 10 cycles, a slight shift towards lower voltage of discharge peaks can already be observed from BE-FEC cells compared to BE cells. While at 1 C rate, the shift towards the higher voltage of charging peaks and lower voltage of discharging peak is more obvious in BE-FEC cells. Meanwhile, to rule out the influence of the polarization in Li metal foil, symmetrical batteries consisting of two identical Li foils and corresponding electrolytes are assembled and tested. As shown in **Fig. S3**, the difference in overpotential between symmetrical cells with BE and BE-FEC is trivial compared to the corresponding NCM90 cells. This indicates the

formation of CEI for BE-FEC could increase the overall polarization, which could cause large capacity loss during cycling, especially at higher rates.

To further test the effect of the FEC additive on the cycle performance of NCM90, a long-term cyclic test was taken within a voltage range of 2.5~4.25 V and 2.5~4.6 V, as it was shown in Fig. 4(e). The cells are cycled at 1 C after the first 6 low-rate (0.1 C) cycles for stabilization. It can be discovered that the BE cell has the highest primary capacity (~205 mAh g^{-1}) within a voltage range of 2.5~4.6 V, while the capacity after 500 cycles (~115 mAh g^{-1}) is the best among all the cases. While for BE-FEC, the specific capacity after 500 cycles with a cut-off voltage of 4.6 V is less than 100 mAh g^{-1}. This can be attributed to the continuous formation of thick LiF-based CEI which leads to high polarization. Interestingly, a different trend can be observed with a cut-off voltage of 4.25 V, where the BE-FEC sample shows higher capacity retention as compared to the BE sample. This can be understood since the Li_2CO_3-based CEI is unstable with BE electrolyte, while the formation of thin LiF-based CEI could help to prevent the phase transition to the rock salt structure. The zoomed-in figure on the first 75 cycles indicates that the discharge capacity of NCM90 fades fastest in BE-FEC within 2.5~4.6 V during the first 75 cycles, followed by BE-4.6V cell, BE-FEC-4.25V cell, and BE-4.25V cell. The capacity fading of early cycles shows a great correlation with the formation of LiF, as the high cut-off voltage of 4.6 V promotes the decomposition of $LiPF_6$ and the FEC additive, which generates more LiF and consumes the Li-ion. For long-term cycles, however, the LiF in CEI tends to retard the capacity fading, due to the surface protection with LiF-based CEI.

Overall, the above study indicates that adding fluorinated components such as FEC could promote the formation of LiF-based CEI, which could help to stabilize the cathode surface at a low rate and low voltage. Meanwhile, at a high rate and high voltage, the decomposition of both $LiPF_6$ and FEC could lead to the formation of thick LiF-based CEI that leads to higher polarization and lower capacity retention. Whereas the decomposition of $LiPF_6$ which forms thin LiF-based CEI for standard electrolyte could also stabilize the cathode surface and leads to higher capacity retention. This proves that the excess LiF is detrimental to the overall battery performance.

Fig. 4. Charge-discharge voltage profiles of NCM90 half-cells evolving throughout the cyclic test (a) with BE at a rate of 0.1 C, (b) with BE-FEC at 0.1C, (c) with BE at 1C, and (d) with BE-FEC at 1C.

To further explore the electrochemical properties of NCM90 cells with BE and BE-FEC electrolytes, we performed EIS and GITT measurements, as shown in **Fig. 5**. The cathodes were charged/discharged at 1C for 150 cycles with different electrolytes and re-assembled with primary BE and new Li foil anode to eliminate the effect of

electrolyte and anode. The EIS curves and the equivalent circuit are shown in Fig. 5(a), while the fitted series resistance R_s and charge transfer resistance R_{ct} are given in Table 1. It can be observed that initially, BE has a larger R_s but a much smaller R_{ct} as compared to the BE-FEC cells, indicating the interface formed by NCM90 soaking in BE has a better charge transfer property whereas the formation of LiF with BE-FEC could largely increase the charge transfer barrier. After 150 cycles, the R_{ct} of CEI in BE cell increases slightly, which could be attributed to the rock-salt layer and LiF-based CEI formed on the interface during charge/discharge, whereas the R_{ct} of CEI in BE-FEC shows a significant drop. This is unexpected, indicating that the mixed interface of LiF and layered structure formed under high potential in BE-FEC, which is observed from HRTEM images, could crack locally under fast charge/discharge, leading to a lower charge transfer resistance.

The voltage drops after stopping charging can intuitively reflect the polarization of NCM90 cathodes, especially the part caused by poor mass transfer kinetics. As is shown in Fig. 5(b), the instant voltage drops after the removal of the charging current are equivalent for BE and BE-FEC throughout the cyclic test (~ 0.15 V at the 150th cycle). This sudden voltage drop is due to the linear response of overpotential and current for ohmic polarization. Since the R_s of BE and BE-FEC cells are similar in magnitude, this similar drop is quite reasonable. However, the voltage after relaxing for 5 min shows a great difference at the 10th cycle. The voltage fading of the BE-FEC cell is about 0.02 V higher than BE cell at the 10th cycle, which increases to about 0.04 V after 150 cycles. This indicates a worse Li^+ diffusion kinetics in the CEI of NCM90

with BE-FEC. GITT measurement was taken to further determine diffusion coefficient

D of Li^+ during the charge/discharge process at the interface after 150 cycles, as it is

shown in Fig. 5(c)-5(d). The log D value of Li^+ in BE cell is overall larger than that in

BE-FEC, which proves that CEI between NCM90 and electrolyte without FEC additive

has a better mass transfer property.
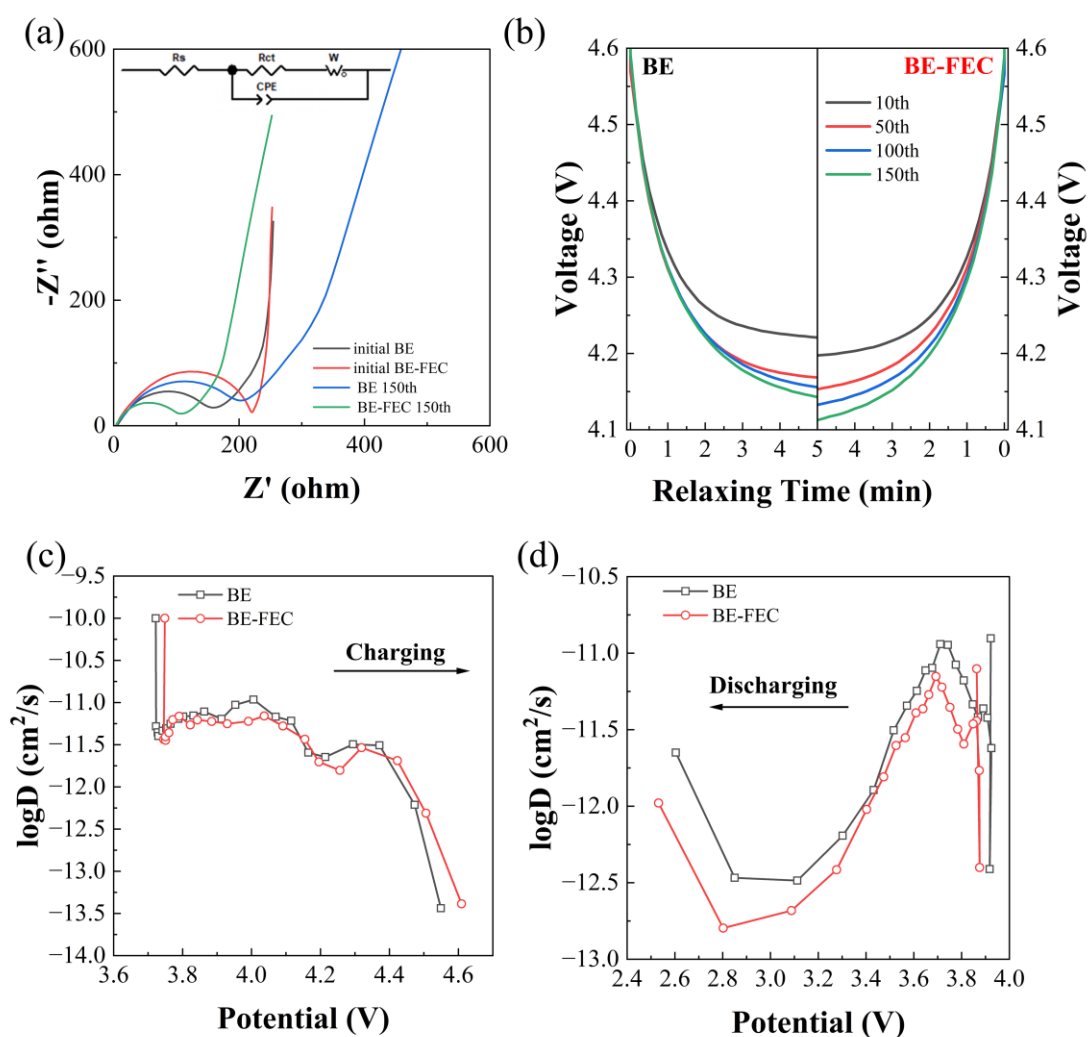
Fig. 5. (a) The electrochemical impedance spectra (EIS) of NCM90 half-cell with BE

and BE-FEC before and after the cyclic test. (b) 5 min relaxing voltage-time profile of

NCM90 half-cell with BE and BE-FEC after charged to 4.6 V at 0.1 C rate. Log D-

potential profile of NCM90 cathode in BE and BE-FEC during (c) charging and (d)discharging calculated from GITT measurement.

Table 1. The fitted series resistance R_s and charge transfer resistance R_{ct}

Cell ID	R_s/ohm	R_{ct}/ohm
Initial BE	7.956	137.5
Initial BE-FEC	4.698	201.5
BE 150th	3.300	152.6
BE-FEC 150th	3.908	87.21

Conclusion

In this work, we investigate the effect of fluorinated electrolytes such as FEC additive on the surface CEI components and electrochemical performances of the nickel-rich NCM90 cathodes. The structural transformations and interface compositions are investigated by XRD, HRTEM, and XPS. Overall, the FEC additive helps generate a CEI with more stable LiF under a relatively low cut-off charging potential and low rate, while Li_2CO_3-based CEI components are formed with standard carbonate electrolytes (BE) which is unstable during cycling. Whereas under a high cut-off potential, LiF-based CEI components are formed even for standard carbonate electrolytes, due to the decomposition of $LiPF_6$. HRTEM and ex-situ XRD studies reveal that rock salt structure is formed with BE while mixed LiF and layered materials

are formed with BE-FEC at the cathode surface. The electrochemical testing indicates that the LiF-based CEI can suppress the degradation of the NCM90 cathode when cycled under low cut-off voltage. However, the abundant LiF generated by both FEC and LiPF6 decomposition at high voltage and high rate will hinder the diffusion of Li^+, thereby increasing the polarization at the interface and hindering the capacity release of nickel-rich NCM90 cathodes after long-term cycling. Meanwhile, LiPF6 decomposition at high voltage could form a thinner LiF layer for BE, which also help to stabilize the cathode surface. This indicates that the role of LiF-based CEI for nickel-rich NCM cathode is complex, and is dependent on the thickness of the CEI. While notably, the fluorinated additives may be detrimental for NCM90 cathodes at high voltage and high rate, due to the formation of excess LiF on the cathode surfaces. We hope this study to spur further interest in the fundamental understanding of CEI formation for high nickel cathodes and electrolyte engineering toward better lithium-ion batteries.

Experimental section

Battery assembly. The cathode was obtained with 80 wt% of NCM90 materials (Lingbo Ronbay New Energy Technology Co., Ltd., China), 10 wt% Ketjen Black (Lion Co., Japan), and 10 wt% polyvinylidene fluoride (PVDF, Arkema, France). All the ingredients were dried in a vacuum at 80 °C for 12 h for further battery assembly. They were grounded for 10 min in an agate mortar to ensure full mixing before dissolving in NMP (99.5%, Rhawn, China) solvent, and consequently stirred using a magnetic stir bar under 800 rpm for 5 h to form a homogenous slurry. It was further

cast on a carbon-coated Al foil and dried at 80°C for 12 h in a vacuum. Then the cathode was pouched into round cathode disks with a radius of 15 mm, calendared under a pressure of 20 MPa, and dried in a vacuum at 80°C for another 4 h to further remove the residual NMP solvent. The standard coin cells were then assembled in Ar filled glovebox. The coin cells were assembled with Li metal anode (China Energy Lithium Co., Ltd., China) as the counter electrode, BE or BE-FEC as the electrolyte, and separator (Celgard Co., Ltd., USA).

Characterizations. Structure characterizations were performed to investigate the phase, morphology, and elemental distributions of cathode materials. Half-cells were first cycled at 0.1 C in a voltage range of 2.5-4.6 V for 2 charging/discharging cycles, then subjected to constant-current constant-voltage (CCCV) charging/discharging at 0.1 C and voltage holding for 1 h. The cathodes were then removed from the half-cells in an Ar-filled glovebox, washed thrice with DMC (>99%, water≤50ppm, Shanghai Macklin Biochemical Technology Co., Ltd., China), and then dried in an Ar atmosphere. Ex-situ XRD (Rigaku SmartLab Diffractometer) was performed with Cu-Kα radiation (λ = 1.54059 Å) to reveal the crystal structure change during the charge-discharge process. Cathodes after cyclic tests were also obtained from the same battery disassembly process above. HRTEM (JEOL JEM-F200) was performed to observe the surface structure of cycled NCM90 cathode. XPS measurement (Thermo Scientific Nexsa) was used to reveal the chemical environment of the NCM90 surface.

Electrochemical tests. EIS was tested using the electrochemical workstation (CHI600 series, USA), with the test frequency range of $0.1\text{-}10^5$ Hz. The cyclic test and GITT

measurement were performed using a Land battery testing station (Wuhan LAND Electronic Co. Ltd., China) in a 25°C incubator. A voltage range of 2.5-4.6 V was used for GITT measurement. For the long-term cyclic test, the first three cycles were tested at 0.1 C, followed by another three 0.3 C cycles and then 1 C cycles.

Acknowledgment

References

1. Deng, D. Li-Ion Batteries: Basics, Progress, and Challenges. *Energy Sci. Eng.* **2015**, 3 (5), 385-418.

2. Li, M.; Lu, J.; Chen, Z.; Amine, K. 30 Years of Lithium-Ion Batteries. *Adv. Mater.* **2018**, 30 (33), 1–24.

3. Ding, Y.; Cano, Z. P.; Yu, A.; Lu, J.; Chen, Z. Automotive Li-Ion Batteries: Current Status and Future Perspectives. *Electrochem. Energy Rev.* **2019**, 2 (1), 1-28.

4. Fan, X.; Wang, C. High-Voltage Liquid Electrolytes for Li Batteries: Progress and Perspectives. *Chem. Soc. Rev.* **2021**, 50 (18), 10486-10566.

5. Tian, C.; Qin, K.; Suo, L. Concentrated electrolytes for rechargeable lithium metal batteries. *Mater. Futures* **2023**, 2, 012101.

6. Yuan, S.; Ding, K.; Zeng, X.; Bin, D.; Zhang, Y.; Dong, P.; Wang, Y. Advanced Non-Flammable Organic Electrolyte Promises Safer Li Metal Batteries: From Solvation Structure Perspectives. *Adv. Mater.* **2023**, 35, 2206228.

7. Xu, K. Li-Ion Battery Electrolytes. *Nat. Energy* **2021**, 6 (7), 763.

8. Liu, Y.; Zhao, C.; Du, J.; Zhang, X.; Chen, A.; Zhang, Q. Research Progresses of Liquid Electrolytes in Lithium-Ion Batteries, *Small* **2023**, 19, 2205315.

9. Hubble, D.; Brown, D. E.; Zhao, Y.; Fang, C.; Lau, J.; McCloskey, B. D.; Liu, G. Liquid Electrolyte Development for Low-Temperature Lithium-Ion Batteries. *Energy Environ. Sci.* **2022**, 15 (2), 550–578.

10. Zhang, H.; Eshetu, G. G.; Judez, X.; Li, C.; Rodriguez-Martínez, L. M.; Armand, M. Electrolyte Additives for Lithium Metal Anodes and Rechargeable Lithium Metal Batteries: Progress and Perspectives. *Angew. Chemie - Int. Ed.* **2018**, 57 (46), 15002–15027.

11. Han, B.; Zhang, Z.; Zou, Y.; Xu, K.; Xu, G.; Wang, H.; Meng, H.; Deng, Y.; Li, J.; Gu, M. Poor Stability of Li_2CO_3 in the Solid Electrolyte Interphase of a Lithium-Metal Anode Revealed by Cryo-Electron Microscopy. *Adv. Mater.* **2021**, 33 (22), 1-10.

12. Kondo, Y.; Abe, T.; Yamada, Y. Kinetics of Interfacial Ion Transfer in Lithium-Ion Batteries: Mechanism Understanding and Improvement Strategies. *ACS Appl. Mater. Interfaces* **2022**, 14 (20), 22706–22718.

13. Chen, Z.; Wang, B.; Li, Y.; Bai, F.; Zhou, Y.; Li, C.; Li, T. Stable Solvent-Derived

Inorganic-Rich Solid Electrolyte Interphase (SEI) for High-Voltage Lithium-Metal Batteries. *ACS Appl. Mater. Interfaces* **2022**, 14 (24), 28014-28020.

14. Takenaka, N.; Bouibes, A.; Yamada, Y.; Nagaoka, M.; Yamada, A. Frontiers in Theoretical Analysis of Solid Electrolyte Interphase Formation Mechanism. *Adv. Mater.* **2021**, 33 (37), 1-15.

15. Qin, Y.; Ren, Z.; Wang, Q.; Li, Y.; Liu, J.; Liu, Y.; Guo, B.; Wang, D. Simplifying the Electrolyte Systems with the Functional Cosolvent. *ACS Appl. Mater. Interfaces* **2019**, 11 (31), 27854-27861.

16. Aurbach, D.; Markevich, E.; Salitra, G. High Energy Density Rechargeable Batteries Based on Li Metal Anodes. The Role of Unique Surface Chemistry Developed in Solutions Containing Fluorinated Organic Co-Solvents. *J. Am. Chem. Soc.* **2021**, 143 (50), 21161-21176.

17. Guo, R. Impact of LiF Particle Morphology on Overpotential and Structure of Li Metal Deposition. *J. Electrochem. Soc.* **2022**, 169, 100523.

18. Schipper, F.; Erickson, E. M.; Erk, C.; Shin, J.-Y.; Chesneau, F. F.; Aurbach, D. Review-Recent Advances and Remaining Challenges for Lithium Ion Battery Cathodes. *J. Electrochem. Soc*. **2017**, 164 (1), A6220-A6228.

19. Zhou, Y.; Hu, Z.; Huang, Y.; Wu, Y.; Hong, Z. Effect of Solution Wash on the Electrochemical Performance of $LiNi_{0.8}Co_{0.1}Mn_{0.1}O_2$ Cathode Materials. *J. Alloys Compd.* **2021**, 888, 161584.

20. Shen, X.; Zhang, X.; Ding, F.; Huang, J. Xu, R.; Chen, X.; Yan, C.; Su, F.; Chen,

C.; Liu, X.; Zhang, Q. Advanced Electrode Materials in Lithium Batteries: Retrospect and Prospect. *Energy Mater. Adv.* **2021**, 1205324.

21. Gao, Y.; Park, J.; Liang, X. Comprehensive Study of Al- And Zr-Modified $LiNi_{0.8}Mn_{0.1}Co_{0.1}O_2$ through Synergy of Coating and Doping. *ACS Appl. Energy Mater.* **2020**, *3* (9), 8978-8987.

22. Xie, Q.; Cui, Z.; Manthiram, A. Unveiling the Stabilities of Nickel-Based Layered Oxide Cathodes at an Identical Degree of Delithiation in Lithium-Based Batteries. *Adv. Mater.* **2021**, 33 (32), 1–14.

23. Zhang, J. N.; Li, Q.; Wang, Y.; Zheng, J.; Yu, X.; Li, H. Dynamic Evolution of Cathode Electrolyte Interphase (CEI) on High Voltage $LiCoO_2$ Cathode and Its Interaction with Li Anode. *Energy Storage Mater.* **2018**, 14, 1–7.

24. Xin, F.; Zhou, H.; Zong, Y.; Zuba, M.; Chen, Y.; Chernova, N. A.; Bai, J.; Pei, B.; Goel, A.; Rana, J.; Wang, F.; An, K.; Piper, L. F. J.; Zhou, G.; Whittingham, M. S. What Is the Role of Nb in Nickel-Rich Layered Oxide Cathodes for Lithium-Ion Batteries? *ACS Energy Lett.* **2021**, 6 (4), 1377–1382.

25. Hu, G.; Tao, Y.; Lu, Y.; Fan, J.; Li, L.; Xia, J.; Huang, Y.; Zhang, Z.; Su, H.; Cao, Y. Enhanced Electrochemical Properties of $LiNi_{0.8}Co_{0.1}Mn_{0.1}O_2$ Cathode Materials Modified with Lithium-Ion Conductive Coating $LiNbO_3$. *ChemElectroChem* **2019**, 6 (18), 4773-4780.

26. Han, B.; Key, B.; Lapidus, S. H.; Garcia, J. C.; Iddir, H.; Vaughey, J. T.; Dogan, F. From Coating to Dopant: How the Transition Metal Composition Affects Alumina Coatings on Ni-Rich Cathodes. *ACS Appl. Mater. Interfaces* **2017**, *9* (47), 41291-41302.

27. Shi, Y.; Kim, K.; Xing, Y.; Millonig, A.; Kim, B.; Wang, L.; Lee, E.; Harrison, C.; Yu, T.; Johnson, D. C.; Lipson, A. L.; Durham, J. L.; Liu, D.; Fister, T. T.; Yu, L.;

Wen, J. Facile and Scalable Dry Surface Doping Technique to Enhance the Electrochemical Performance of $LiNi_{0.64}Mn_{0.2}Co_{0.16}O_2$ cathode Materials. *J. Mater. Chem. A* **2020**, *8* (38), 19866–19872.

28. She, S.; Zhou, Y.; Hong, Z.; Huang, Y.; Wu, Y. Surface Coating of NCM-811 Cathode Materials with g-C_3N_4 for Enhanced Electrochemical Performance. *ACS Omega* **2022**, 7 (28), 24851-24857.

29. Schipper, F.; Bouzaglo, H.; Dixit, M.; Erickson, E. M.; Weigel, T.; Talianker, M.; Grinblat, J.; Burstein, L.; Schmidt, M.; Lampert, J.; Erk, C.; Markovsky, B.; Major, D. T.; Aurbach, D. From Surface ZrO_2 Coating to Bulk Zr Doping by High Temperature Annealing of Nickel-Rich Lithiated Oxides and Their Enhanced Electrochemical Performance in Lithium Ion Batteries. *Adv. Energy Mater.* **2018**, 8, 1701682.
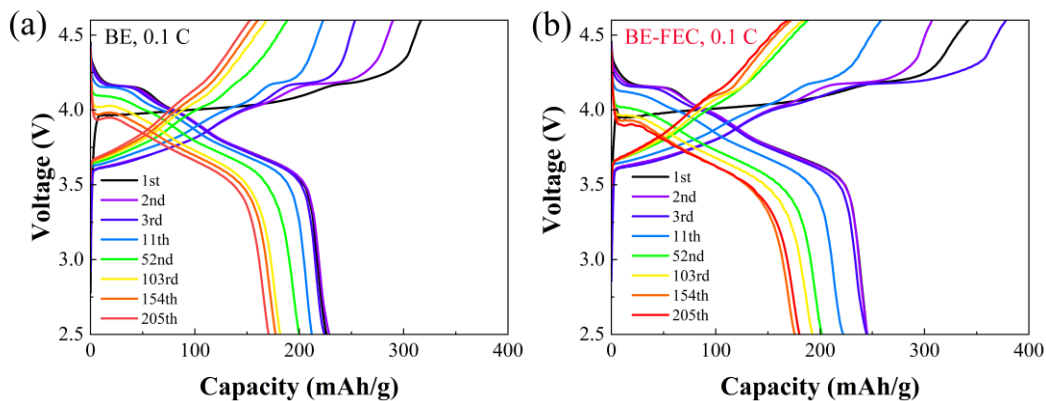
Fig. S1. Charge-discharge voltage profiles of NCM90 half-cells evolving throughout cyclic test at a rate of 0.1C (a) with BE, (b) with BE-FEC.
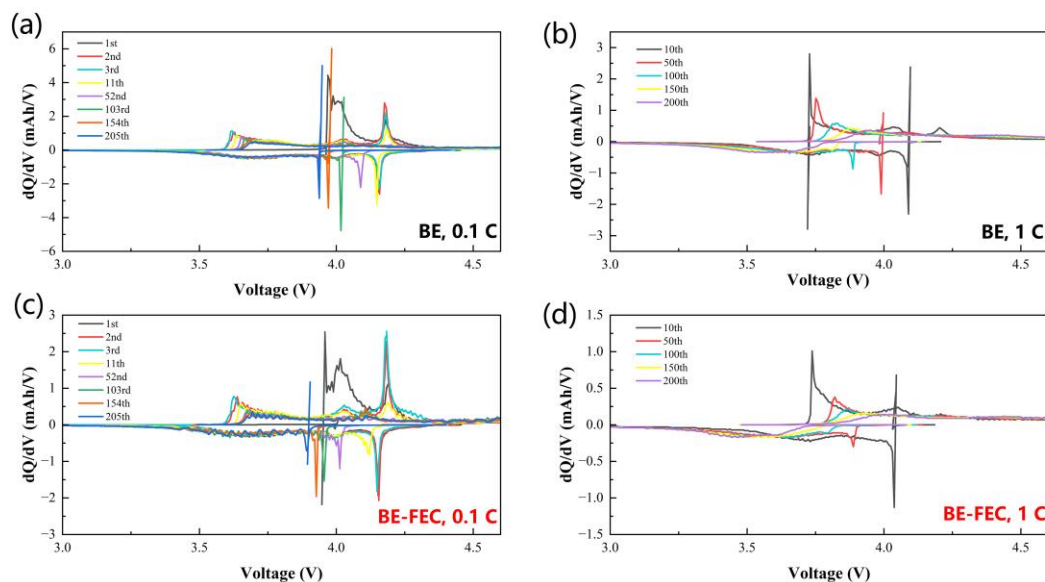
Fig. S2. Differential capacity curves of NCM90 half-cells evolving throughout cyclic test (a) with BE at a rate of 0.1 C, (b) with BE at 1C, (c) with BE-FEC at 0.1C, and (d) with BE-FEC at 1C.
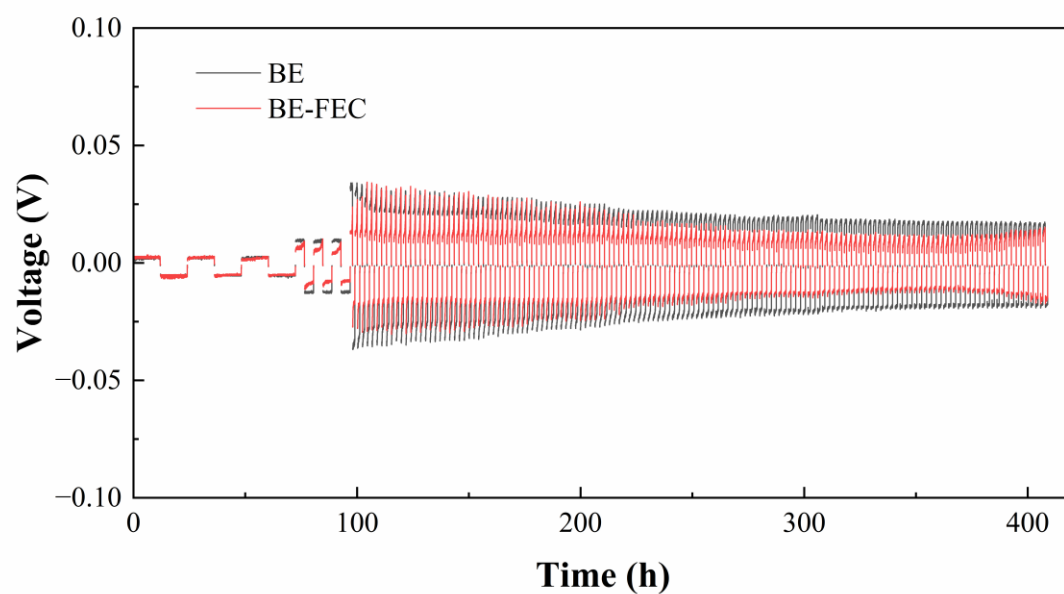
Fig. S3 Voltage-time profile of symmetrical batteries consisting of two identical Li foils and BE and BE-FEC, respectively. The test time is equivalent to the time for 150 cycles at 1 C of NCM90 cathode.